NUMERICAL SIMULATION OF FLOW DYNAMICS IN THE PERIODIC REGIME IN AN IDEALIZED THERMOACOUSTIC ENGINE

L. Ma[1], *C. Weisman*[1], *D. Baltean-Carlès*[1],
I. Delbende[1], *L. Bauwens*[2]

[1] *Sorbonne Universités, UPMC Univ Paris 06, UFR919, 75005, Paris,
LIMSI-CNRS, UPR 3251, rue John von Neumann, 91405 Orsay Cedex, France*
[2] *University of Calgary, Calgary Alberta T2N 1N4, Canada*

Flow dynamics in the stack and heat exchangers of a standing wave thermoacoustic engine is studied using two-dimensional direct numerical simulations. The numerical approach is based on asymptotic coupling in the low Mach number limit of a nonlinear dynamic model in the active cell with linear acoustics in the resonator. Computed results of the initial amplification and of the periodic regime eventually reached are shown. For the former, results show the existence of a critical temperature for which the system becomes unstable so that the engine starts, which is strongly dependent upon the load. Analysis of the results in the periodic regime shows the importance of vortex dynamics and the role of vortex shedding at sharp heat exchanger corners.

Introduction. A simplified model of a loaded thermoacoustic engine consists of a long tube closed at one side and loaded at the other side, inside which the active cell is placed. The active cell comprises a stack of parallel plates placed between two heat exchangers. One heat exchanger is connected to a hot source and the other to a cold source. The combined effect of pressure fluctuations and oscillating heat exchange in the boundary layers on the stack plates provides a heat engine effect [1–3]. A multiple scale formulation allows for the global compressible flow problem to be reduced to a dynamically incompressible problem in the active cell, with boundary conditions obtained from linear acoustics in the resonator. The details of this analysis are found in [4, 5]. In the literature, there are few studies dedicated to nonlinear hydrodynamics inside the active cell. The purpose of this paper is to show and analyze numerical results on flow dynamics in the periodic regime, such as instability and vortex dynamics. After a brief introduction of the model and numerical method, the computed results of the periodic regime are presented and discussed in two steps: first, the influence of the load on the onset temperature and saturation is presented, validating the choice of the load value. Then, the flow patterns, temperature field and vorticity field are analyzed and a possible mechanism of the observed instability is discussed qualitatively.

1. Physical model. The geometry consists of a long resonator with length L_{res}, within which an active cell of characteristic stack length L_{s} is placed. The active cell consists of a stack of parallel plates and two heat exchangers (heater and cooler). The heater and the cooler are also made from parallel plates. We assume vertical periodicity, so that the simulation can be reduced to a domain consisting of two half-plates and the space between them, and the corresponding fraction of the resonator cross-section. The active cell is short compared to the resonator length, therefore, two characteristic length scales are to be considered, L_{res} and L_{s}. The geometry of the entire resonator is shown in Fig. 1 (top). The resonator dead end is located at $\hat{x} = -l_{\mathrm{L}}$, while the other end consists of a load modelled as a real impedance f at the fixed location $\hat{x} = l_{\mathrm{R}}$, with $p(l_{\mathrm{R}}, t) = f u(l_{\mathrm{R}}, t)$. The active cell is considered as a discontinuity section positioned at $\hat{x} = 0$.

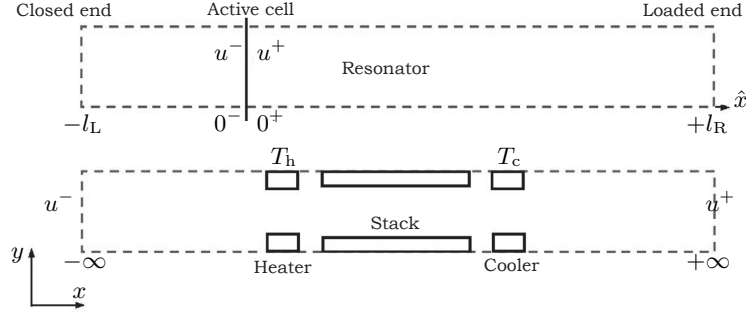L. Ma, C. Weisman, D. Baltean-Carlès, I. Delbende, L. Bauwens

Fig. 1. Geometry of the linear acoustic system (top) and of the active cell (bottom).

As to the stack scale, the geometry of the active cell is shown in Fig. 1 (bottom) and boundaries with the resonator are located at infinity on the scale associated with the active cell. That represents the simulation domain. In the current case, the length is $5L_s$ and the height is H.

The multiple scale formulation is obtained with a perturbation asymptotic method described in detail elsewhere [4, 5]. Key assumptions are that velocities are small compared with the speed of sound, and that the flow sweeps a length of the order of the length of the stack. These assumptions lead to a reference Mach number $M = L_s/L_{res}$. Under these assumptions, the flow in the resonator is characterized by lossless linear acoustics with all dissipation concentrated at the loaded end.

The flow in the active cell is described by a nonlinear dynamically incompressible model.

In the heat exchangers and stack, at leading order and at order M, the momentum leads to $\nabla p^{(0)} = 0$ and $\nabla p^{(1)} = 0$ (here the superscripts characterize the magnitude of the pressure contribution in a power series expansion in the reference Mach number M). Momentum at order M^2 plus leading order conservation of mass and energy result in:

$$\frac{\partial \rho}{\partial t} + \nabla.(\rho \mathbf{u}) = 0$$
$$\frac{\partial(\rho \mathbf{u})}{\partial t} + \nabla.(\rho \mathbf{u} \otimes \mathbf{u}) = -\nabla p^{(2)} + \frac{1}{Re}\nabla.\tau \qquad (1)$$
$$\rho\left[\frac{\partial T}{\partial t} + (\mathbf{u}.\nabla)T\right] = \frac{1}{Pe}\nabla^2 T$$

in which the thermodynamic properties have been scaled by suitable reference values, such that $p^{(0)} = \rho T = 1$. The stress tensor $\tau = [\nabla \mathbf{u} + (\nabla \mathbf{u})^t - \frac{2}{3}(\nabla.\mathbf{u})\mathbf{I}]$ and the reference Reynolds and Péclet numbers are based upon the reference velocity, the stack length L_s, viscosity and conductivity at the reference state. In the solid plates (stack and heat exchanger plates), the conduction equation is

$$\frac{\partial T}{\partial t} = \frac{1}{Pe_s}\Delta T, \qquad (2)$$

with $Pe_s = Pe\,\alpha_{ref}/\alpha_s$, where α_{ref} and α_s are the thermal diffusivities at the reference state, respectively, in the fluid and in the solid.

In the heat exchangers and stack, $\nabla p^{(1)} = 0$, so that they are transparent to acoustic pressure, which is then the same on both sides. Integrating the energy

equation over the heat exchangers and stack results in

$$(u^- - u^+)H + \frac{1}{\text{Pe}} \int \nabla T \cdot \mathbf{n} \mathrm{d}s = 0, \tag{3}$$

with H being the height of the simulation domain, and u^-, u^+ the velocities at locations x_L and x_R. In the local scaling, $x_\mathrm{L} \to -\infty$ and $x_\mathrm{R} \to +\infty$, while in the scaling that describes resonator acoustics they correspond, respectively, to $x = 0^-$ and $x = 0^+$. Velocities u^+ (resp. u^-) have the same values in both problems. This completes the boundary conditions [4, 5].

At solid boundaries, the continuity of temperature and heat flux and no-slip condition are imposed. A temperature $T = T_\mathrm{h}$ is imposed on the heater plates, and $T = T_\mathrm{c}$ is also imposed on the cooler plates. In the stack plates, the heat conduction equation is solved. All active cell boundaries other than the heat exchanger walls are considered adiabatic.

Matching these two solutions in the standard way provides appropriate boundary conditions to the flow inside the heat exchanger section, depending of the impedance value at the load end. From the standpoint of resonator acoustics, the heat exchanger section is transparent to pressure but provides a source of volume, as a result of the thermoacoustic effect.

2. Numerical solution. The numerical solution is based upon a finite volume code solving the Navier–Stokes equations under the low Mach number assumption [6]. The code originally was developed for non-Boussinesq convection. It can handle density and temperatures varying at leading order, together with spatially uniform pressure fluctuations at up to leading order.

Diffusion is solved implicitly and advection is explicit. Accuracy is second-order in both space and time. On both sides of the lossless resonator, acoustics can be expressed as the combination of two plane waves that move respectively left and right at the speed of sound. The boundary conditions at both tube ends determine a relationship between the incoming and the outcoming Riemann invariants. These are carried on characteristics along the tube. The boundary conditions at each end of the active cell correspond to the value of the arriving Riemann invariant, which is thus functions of the outgoing Riemann variable at an earlier time. The acoustic pressure does not appear in the formulation for the active cell, but it affects the Riemann variables hence the boundary conditions.

A Cartesian regular two-dimensional mesh of the active cell is used in the current work (4096×64 grid points, i.e. 9 grid points across the stack half-plate width, and 37 grid points along the gap between the heat exchanger and the stack). The numerical calculation is performed with the following initial condition: a random noise for the velocity field in the whole resonator and a steady state heat conduction condition for the temperature field inside the active cell and a constant temperature in the resonator (T_h for the hot part and T_c for the cold part). In order to satisfy a stability criterion ($\text{CFL} = 0.025$), the time step must be reduced with the increased horizontal velocity, so that from the initial state to the periodic regime, the whole simulation could be extremely long (about 400 reference acoustic periods), with 200 (initial amplification) to 10 000 (periodic regime) time steps per reference acoustic period.

3. Results.
3.1. Reference configuration. Results were obtained for an existing thermoacoustic engine [7]. The active cell was inserted in a long resonator tube closed at both ends. Viscous dissipation inside the resonator plays the role of the load.

Table 1. Geometry and operating conditions.

L_{res} [mm]	L_{s} [mm]	H [mm]	L_{g} [mm]	p_0 [kPa]	T_{h} [K]	t_{ac} [ms]
1000.0	35.0	1.06	1.54	44.0	351.6	1.0

The experiment used helium under pressure $p_0 = 44\,\text{kPa}$, and the cold temperature was taken as the reference temperature $T_{\text{c}} = 293\,\text{K}$. The reference acoustic time t_{ac} was approximately equal to $1\,\text{ms}$. All parameters of the experimental configuration are listed in Table 1. The gap L_{g} between the stack and the heat exchangers was arbitrarily chosen to be equal to twice the plate spacing.

Analysis of the numerical results for initial amplification shows that the load
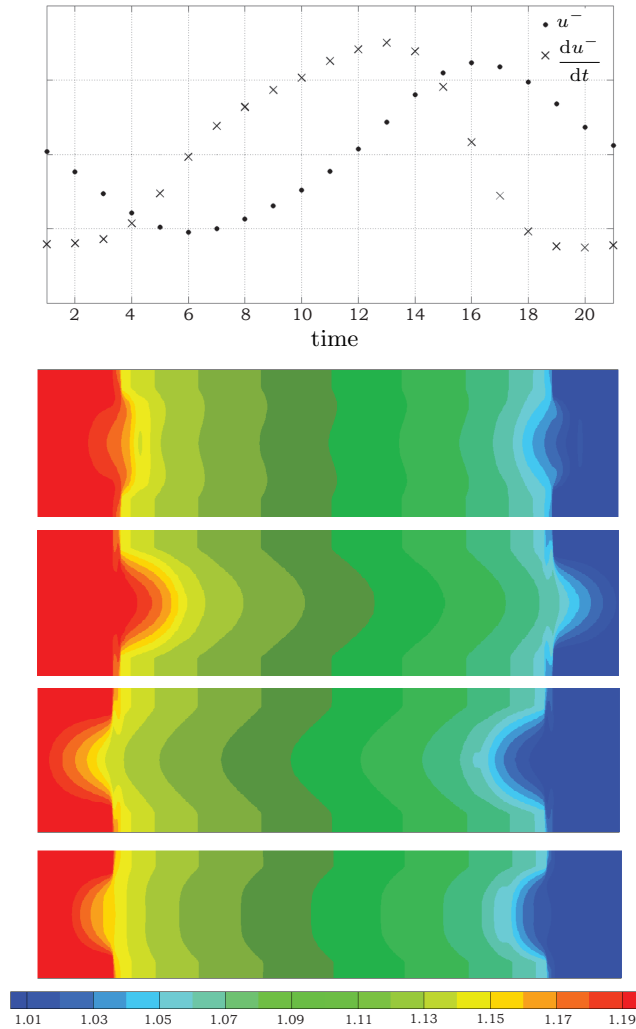

Fig. 2. Top: time evolution of acceleration and velocity at the left entrance of the simulation domain, evolution over one acoustic period, evenly spaced selected times labelled from 1 to 21.. Bottom: the temperature field over the entire simulation domain at times 8, 12, 16, 21 (top to bottom). Color code shown at bottom.

plays an important role in the onset of a thermoacoustic engine. For a given value of the load f and for each acoustic mode, there is a corresponding critical heater temperature. The limit when f is infinite corresponds to a closed end and the limit when f is zero corresponds to an open end. In order to validate the load model, we identified the load value corresponding to a given experimental setup $p_0 = 44\,\text{kPa}$ and $T_\text{h} = 662\,\text{K}$ from the experimental stability curve of the fundamental mode [7]. We obtained a load value of $171.36\,\text{MPa·s/m}^3$. Numerical simulation for that case indicated that the first mode (i.e. the fundamental) was the most unstable, which is in agreement with the experiment.

When the heater temperature was further increased for the same mean pressure value, the numerical simulation with the same load value gave the next critical heater temperature $T_\text{h} = 820\,\text{K}$, and both modes 1 and 2 were unstable, again in agreement with experimental results [7].

To study the periodic regime for a given value of f, we had to choose a heater temperature just above the critical value. By trial and error, we have found that high values of the heater temperature (for example, $T_\text{h} = 743\,\text{K}$) require long numerical calculations until obtaining a saturated regime. Therefore, the previous load value is not suitable. Numerical experiments showed that, in order to obtain the periodic regime faster, we had to choose a higher f. Here for a load of $1523.2\,\text{MPa·s/m}^3$ and for the same mean pressure, we obtained a critical heater temperature $T_\text{h} = 345.7\,\text{K}$. The periodic regime was obtained for $T_\text{h} = 351.6\,\text{K}$. The entire simulation took about 160 hours CPU time on an INTEL XEON.

3.2. Periodic regime. In this section, the periodic regime is discussed in detail. All results are presented below using dimensionless values.

Fig. 2 (top) shows the time evolution of the acceleration and the velocity at the left entrance of the simulation domain over one acoustic period. Fig. 2 (bottom) shows the temperature field over the entire active cell at selected times during the period. Due to the presence of a gap between the heat exchangers and the stack, the temperature gradient along the stack is only 50% of the maximum temperature gradient $\Delta T / L_\text{s}$. The entire acoustic period is divided into 21 equal steps. There is an interplay between the acceleration of the flow and the longitudinal temperature gradient, resulting in an instability of the Rayleigh–Taylor type, similar to the situation, where a heavy, cold fluid is situated above a hotter, lighter fluid in a gravitational field, resulting in fingering. Between the entrance and the exit, densities differ because of the longitudinal temperature gradient imposed through the heat exchangers. If the hot light fluid is pushing the cool heavy flow, the instability occurs. Conversely, when the acceleration switches its direction, the flow restabilizes. Here, the flow acceleration is due to acoustics in the resonators. However, the situation is more complex; changes in cross-section also induce acceleration/deceleration, but even that effect is made more complex because of the significant role of vortices, as the results below show.

The evolution during the acoustic period of acceleration and the velocity at the entrance and exit of the simulation domain are shown in Fig. 3. The values at the entrance and exit, while differing in principle, are almost equal in the current case.

Fig. 4 shows the instantaneous temperature field and the streamlines (left column) and the corresponding vorticity field (right column) between the stack and the heater at four different times (8, 12, 14, 16) within the acoustic period. As expected, one can observe that vortices are generated between the heater and the stack, where sudden changes of the cross-section occur. Likewise, vortices can be also observed at the inlet and outlet of the heat exchangers and between the stack and the cooler (not shown in Fig. 4). All vortices are symmetrical in the
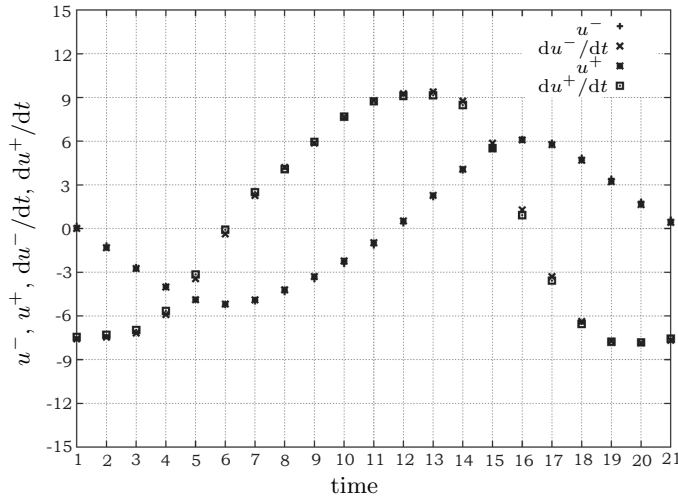
605

L. Ma, C. Weisman, D. Baltean-Carlès, I. Delbende, L. Bauwens

Fig. 3.   Acceleration and velocity at the entrance and exit of the simulation domain, evolution over the acoustic period, times 1 to 21.

active cell. From time 8 to time 12, the vortices accumulate and roll into the gap between the heater and the stack as long as the flow velocity is significant. Time 8 corresponds to the beginning of flow reversal, as the two vortices grow and move out of the gap. At time 12, the vortices move toward the center of the channel. From time 12 to time 14, the vortices are sucked outside of the gap area and move toward the right, and recirculation vortices become visible in the boundary layer. This continues between time 14 and 16, and finally the plate spacing between two plates of the stack can be divided into two boundary layer regions and the domain outside it. The boundary layer regions absorb the two vortices close to the stack plates, and the vortices disappear gradually.

These features can actually be observed on both sides of the stack; both sides are qualitatively very similar, but at different temperature levels.

4. Conclusions. Direct simulation was performed of a complete thermoacoustic engine for which experimental data are available [7]. A multiple scale formulation allows for the global compressible flow problem to be reduced to a dynamically incompressible problem in the heat exchangers, with boundary conditions obtained from linear acoustics in the resonator. In order to obtain the saturation faster, a high load value was used, leading to the lower onset temperature.

Results in the transient regime, corresponding to early amplification, show that the initial growth rate is strongly dependent on the load applied to the system. For the stationary regime, from the simulation, visualization data of the flow near both heat exchanger ends were extracted. The resulting figures exhibit two main features: instability and vortex dynamics. Since due to the temperature difference between the hot and cold heat exchangers, a longitudinal temperature gradient exists, and since both the oscillating flow and the cross-section changes result in periodic acceleration of the oscillating flow, one should expect that during part of the cycle the combined effect of these two features will result in a destabilizing/restabilizing mechanism of the Rayleigh–Taylor type. Indeed, the results above evidence of a strong instability, present only during part of the cycle.

Likewise, the vortex dynamics associated with cavities, corners and step-like cross-section changes under oscillating flow show interesting features that are observed in the results, interplaying with temperature gradients and accelerations.
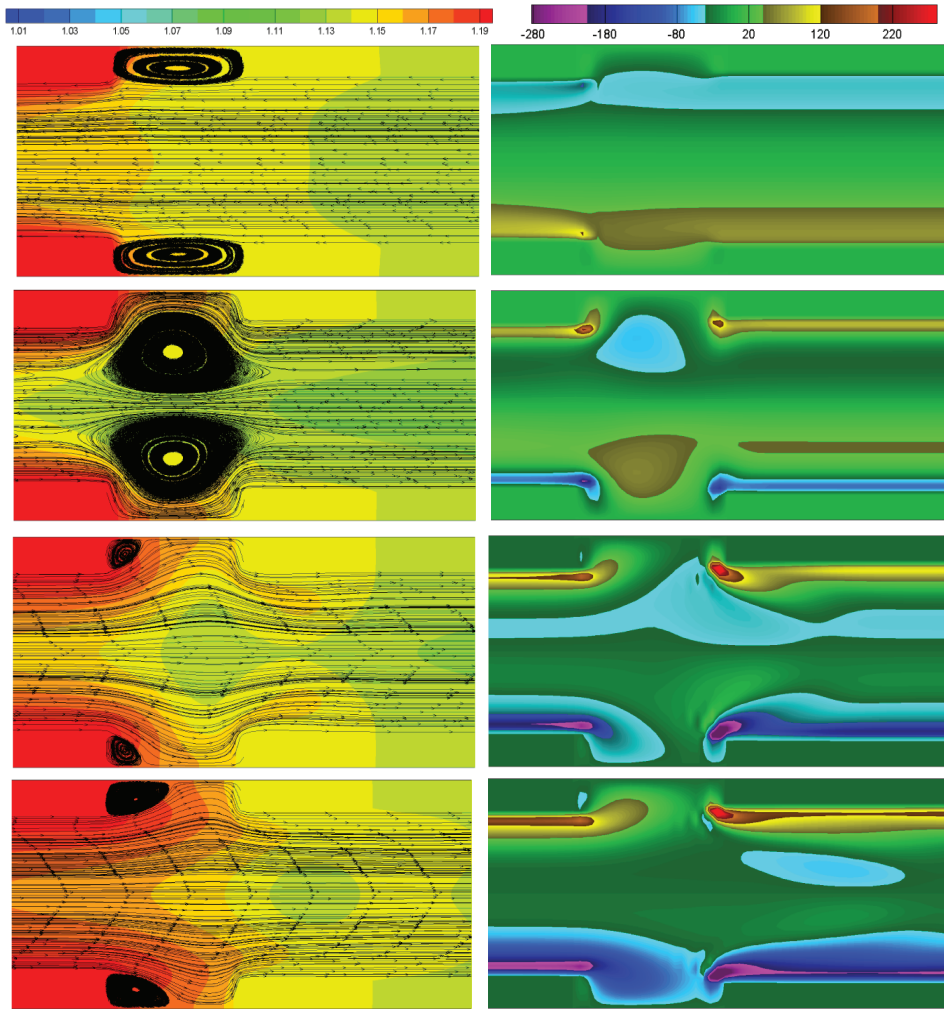
Fig. 4.   Temperature and streamlines (left) and vorticity fields (right) between the hot heat exchanger and the stack at four different times (8, 12, 14, 16 from top to bottom, using scales shown on top).

While the current results are mostly qualitative, they potentially will have a significant impact on heat transfer and losses, not only in thermoacoustic devices as the one that was simulated, but more generally, in alternating flow devices subject to pressure fluctuations, temperature gradients and oscillating accelerations. Thus, the results are also relevant to Stirling engines and pulse-tube cryocoolers, where it would also be good practice to avoid as much as possible abrupt changes of cross-section, where the boundary layer detaches and sheds vortices.

References

[1] N. ROTT. Damped and thermally driven acoustic oscillations in wide and narrow tubes. *Z Angew Math Phys.*, vol. 20 (1969), pp. 230–243.

[2] G.W. SWIFT Thermoacoustic engines. *J. Acoust. Soc. Am.*, vol. 84 (1988), pp. 1145–1180.

[3] L. BAUWENS. Oscillating flow of a heat-conducting fluid in a narrow tube. *J. Fluid Mech.*, vol. 324 (1996), pp. 135–161.

[4] O. HIRECHE, C. WEISMAN, D. BALTEAN CARLÈS, P. LE QUÉRÉ, M.X. FRANÇOIS, L. BAUWENS. Numerical model of a thermoacoustic engine. *Comptes Rendus Mécanique*, vol. 338 (2010), pp. 18–23.

[5] O. HIRECHE, C. WEISMAN, D. BALTEAN CARLÈS, P. LE QUÉRÉ, L. BAUWENS. Multiple scale analysis and simulation of thermoacoustic engines. *J. Acoust. Soc. Am.*, vol. 128 (2010), pp. 3438–3448.

[6] P. LE QUÉRÉ, R. MASSON, P. PERRO. Chebyshev collocation algorithm for 2D non-Boussinesq convection. *J. Comp. Physics*, vol. 103 (1992), pp. 320–335.

[7] A.A. ATCHLEY, F.M. KUO. Stability curves for a thermoacoustic prime mover. *J. Acoust. Soc. Am.*, vol. 95 (1994), pp. 1401–1404.